energies

MDPI

Article

Well Testing Methodology for Multiple Vertical Wells with Well Interference and Radially Composite Structure during Underground Gas Storage †

Hongyang Chu [1,2,3,*], Tianbi Ma [4,5], Zhen Chen [1], Wenchao Liu [1] and Yubao Gao [1]

[1] School of Civil and Resources Engineering, University of Science and Technology Beijing, Beijing 100083, China
[2] Harold Vance Department of Petroleum Engineering, Texas A&M University, College Station, TX 77843, USA
[3] State Key Laboratory of Petroleum Resources and Prospecting, China University of Petroleum, Beijing 102249, China
[4] Petroleum Exploration and Production Research Institute, SINOPEC, Beijing 100083, China
[5] Department of Geosciences, The University of Tulsa, Tulsa, OK 74104, USA
* Correspondence: hongyangchu@126.com or hongyangchu@ustb.edu.cn; Tel.: +86-15600277900
† This paper is an extended version of our paper published in the SPE Annual Technical Conference and Exhibition, Houston, TX, USA, 3–5 October 2022. Paper Number: SPE-210187-MS.

Abstract: To achieve the goal of decarbonized energy and greenhouse gas reduction, underground gas storage (UGS) has proven to be an important source for energy storage and regulation of natural gas supply. The special working conditions in UGS cause offset vertical wells to easily interfere with target vertical wells. The current well testing methodology assumes that there is only one well, and the interference from offset wells is ignored. This paper proposes a solution and analysis method for the interference from adjacent vertical wells to target vertical wells by analytical theory. The model solution is obtained by the solution with a constant rate and the Laplace transform method. The pressure superposition is used to deal with the interference from adjacent vertical wells. The model reliability in the gas injection and production stages is verified by commercial software. Pressure analysis shows that the heterogeneity and interference in the gas storage are caused by long-term gas injection and production. As both the adjacent well and the target well are in the gas production stage, the pressure derivative value in radial flow is related to production rate, mobility ratio, and 0.5. Gas injection from offset wells will cause the pressure derivative to drop later. Multiple vertical wells from the Hutubi UGS are used to illustrate the properties of vertical wells and the formation.

Keywords: underground gas storage; multiple vertical wells; flow behavior; well interference; case study; analytical model

check for updates

Citation: Chu, H.; Ma, T.; Chen, Z.; Liu, W.; Gao, Y. Well Testing Methodology for Multiple Vertical Wells with Well Interference and Radially Composite Structure during Underground Gas Storage. *Energies* **2022**, *15*, 8403. https://doi.org/10.3390/en15228403

Academic Editor: Manoj Khandelwal

Received: 6 October 2022
Accepted: 4 November 2022
Published: 10 November 2022

Publisher's Note: MDPI stays neutral with regard to jurisdictional claims in published maps and institutional affiliations.

Copyright: © 2022 by the authors. Licensee MDPI, Basel, Switzerland. This article is an open access article distributed under the terms and conditions of the Creative Commons Attribution (CC BY) license (https://creativecommons.org/licenses/by/4.0/).

1. Introduction

To pursue carbon-peaking and carbon-neutral goals, as well as meet the cycling energy demand on the electricity power grids, the major countries around the world typically employ large-scale energy storage systems [1]. These energy storage systems include pumped hydropower, compressed air, and UGS. In this context, UGS has been proven to be the most commercially mature large-scale energy storage technology and it has been implemented in many countries including China [2]. Natural gas is a fossil fuel with more potential for energy conversion and clean emissions than liquid petroleum [3,4]. The molecular formula of natural gas makes its combustion products virtually free of sulfur, dust, and other harmful substances, and it produces significantly less CO_2 than other fossil fuels. In addition, due to the recovery, transportation, and processing costs of natural gas, it is an attractive alternative to petroleum energy in the oil and gas industry [5]. Thus, from 2008 to 2018, natural gas consumption increased by 28.35% [6,7].

Although China has abundant natural gas resources, the supply of and demand for natural gas have been affected in the long term by technology and equipment limitations. In 2018, 42.9% of China's natural gas consumption was imported from overseas [8]. The limitations of the natural gas market also include seasonal and geographical factors. Most of China's natural gas reserves are located in the western region, while the principal areas of natural gas consumption are mostly developed cities along the eastern coast. Additionally, heating is one of the important purposes of natural gas, resulting in a much larger natural gas demand in winter than that in summer. To resolve these incongruities in the natural gas market, UGS is an important part of the natural gas industry [9].

Compared with the salt cavern type of UGS, the porous reservoir type of UGS has the advantages of a short UGS construction period and low operating cost. The limitation is that the stored gas cannot be recovered completely and the recovered gas in the surface requires further processing process. The injection and withdrawal rates in salt cavern type of UGS are fast, and most of the stored gas can be recovered. However, the total gas storage capacity in the salt cavern type of UGS is lower, and this UGS type has a higher probability of leakage risk. The treatment of brine in salt caverns requires additional technology. Therefore, porous reservoirs are more suitable large-scale storage sites. As shown in Table 1, the screen criteria include caprock lithology, tectonic activity, reservoir type, depth, and pore volume of the reservoir. The number of UGS facilities, working gas capacity, and maximal withdrawal rates of the porous reservoir (depleted oil and gas reservoir) type of UGS all largely dominate the total number of UGSs in North America, Europe, Commonwealth of Independent States (CIS), Middle East, and Asia–Oceania, as given in Table 2. In contrast to the recovery processes in these oil and gas reservoirs, the injection/production process in the UGS has the features of high rate, continuous injection/production in a short period, and collective well shut-in in a period [10,11]. The natural gas composition in UGS is related to the porous media type. As the UGS type is the acid gas reservoir, the acid gas content of the produced gas will gradually decrease. In an injection–withdrawal cycle, the acid gas content in the gas composition will increase with the increase in produced gas volume [12]. For the UGSs of the condensate gas reservoir type, the injected gas can evaporate and extract the condensate oil in the formation. This effect becomes significant with the increase in gas injection pressure. With the increase in the injection–withdrawal cycle, the contents of C2, C3 and C7+ components in the produced gas show a trend of first increasing and then decreasing [13]. These unconventional operating and composition conditions result in the unique flow behavior of UGS.

Table 1. The screen criteria for the depleted oil and gas reservoir type of UGS (modified from Lewandowska-Śmierzchalska et al. [14]).

	Caprock Lithology	**Tectonic Activity**	**Reservoir Type**	**Depth**	**Pore Volume of Reservoir**
Change from the most suitable type to the unsuitable type	Clay rock, clay shale, calcium sulfate rock, and salt rock	No faults	Gas reservoir	Large	Large
	Mudstone and mud shale	Single independent fault	Gas and oil reservoir	Medium	Medium
	Sandstones and siltstones	Plenty of faults in basement			
	Clay sandstone, limestone, and dolomite	The fault terminates in caprock			
	Sandstones	The fault extends to caprock	Oil reservoir	Small	Small

Table 2. The percentage of the depleted oil and gas reservoir type of UGS in the total number of UGSs (modified from Cedigaz [15]).

	Number of UGS Facilities		Working Gas Capacity		Max. Withdrawal Rates	
Regions	**Salt Caverns**	**Porous Reservoir**	**Salt Caverns**	**Porous Reservoir**	**Salt Caverns**	**Porous Reservoir**
North America	10%	90%	9%	91%	26%	74%
Europe	33%	67%	17%	83%	36%	64%
CIS	6%	94%	1%	99%	3%	97%
Middle East	0%	100%	0%	100%	0%	100%
Asia–Oceania	4%	96%	2%	98%	1%	99%
World Total	14%	86%	8%	92%	24%	76%

Conventional well testing studies are limited to single wells [16]. Multi-well testing mostly is within the scope of interference or pulse tests [17–20]. Interference testing typically requires one well to be active and the other well to be shut in to measure the pressure signal produced by the active well [21]. It is usually used to determine the degree of connectivity between wells or directional permeability. As adjacent wells are producing or injecting, Warren and Hartsock [22] first used an asymptotic approximation solution to describe interference between two production wells in an infinite reservoir. Onur et al. [23] proposed an analytical model for pressure buildup tests in multi-well systems with interference. A limitation of their model is that the multi-well system must achieve quasi-steady-state flow before well shut-in. Fokker and Verga [24] proposed a semi-analytical productivity test model that can consider vertical wells and horizontal wells. This method is not only suitable for oil and gas reservoirs but also "automatically" considers well interference. Aiming at the well interference caused by the adjacent well's water injection, Lin and Yang [25] established a well test model with an adjacent well's water injection by applying the material balance equation and superposition. Izadi and Yildiz [26] used a semi-analytical method to establish a transient model that could consider the multi-well system and natural fractures. For tight carbonate gas reservoirs, Wei et al. [27] proposed a multi-well model for hydraulically fractured wells. Chu et al. [28,29] proposed a semi-analytical model for multiple fractured horizontal wells with well interference. Their target domains include hydraulic fractures, natural fractures, and matrices in unconventional reservoirs. The well testing data of Hutubi UGS show that the well interference is serious [30]. Abnormal rising or falling characteristics appear in the late well testing data. Conventional single-well models cannot match field data from Hutubi UGS. The reason is that it violates the physical assumptions in single-well model (the study domain in single-well models contains only one well). The typical flow behaviors including the effects of well interference in UGS are still unclear. The unique flow behavior in UGS leads to limitations in storage volume calculation and energy storage capacity evaluation.

To fill these gaps, this paper uses an analytical method to establish transient models for the multi-well system with interference in the UGS. First, the governing equation for the multi-well system in a dimensionless domain was constructed. Laplace transforms were used to obtain the basic pressure solution for each well in the multi-well system. A model for the target well was further extended from a homogeneous model to a radially composite model to account for the continuing injection/production process in UGS. Adjacent gas injection/production interference in UGS is "automatically" taken into account by pressure superposition. We used commercial numerical simulators to verify the reliability of the proposed model under different operating conditions. We used flow regime and sensitivity analysis to describe typical flow behavior in UGS. We present a case study from the Hutubi UGS to further illustrate the model practicability. This work provides useful guidelines for storage volume calculation in UGS, energy storage capacity evaluation, and well location optimization.

The innovations of this work include the following: (1) a new analytical model of a multi-well system with well interference and radially composite structure is proposed;

(2) the unique flow regions in UGS are elucidated by sensitivity analysis; (3) a field case from the largest Hutubi UGS in China shows the method practicality.

2. Methodology

2.1. Physical Model

Figure 1a shows the technological process of a depleted oil and gas reservoir used for UGS. The storage process of UGS usually includes long-distance pipelines, filters, metering equipment, a compressor station, a cooler, and porous media. For gas injection process, it includes a heating device, dehydration equipment, metering equipment, and pipelines. Our research objectives mainly focus on the gas flow and storage behavior in porous media. Vertically, the anticline traps can ensure the integrity of UGS. The region of the entire UGS formation is bounded, and the properties of the boundary can be regarded as irregular. As the UGS is a depleted oil and gas reservoir, a large number of vertical wells are distributed in it. These wells can be used as production wells during gas storage, injection wells during gas injection, and monitoring wells during shut-in. The reservoir medium of the UGS can be considered a continuous homogeneous model or a dual-medium model proposed by Warren and Root (1963), as given in Figure 1b. Other assumptions are as follows:

(1) The initial pressure and the properties of the UGS are uniformly distributed.

(2) The UGS has closed top–bottom boundaries, and the outer boundary is irregular and closed.

(3) Gas flow in the UGS is single-phase and compressible and obeys Darcy's law.

(4) The thickness of the UGS is constant and the vertical well penetrates the formation completely.

(5) The effects of temperature and gravity on gas flow in UGS are negligible.

(6) Injection into or production from wells in the multi-well system is at a constant rate.

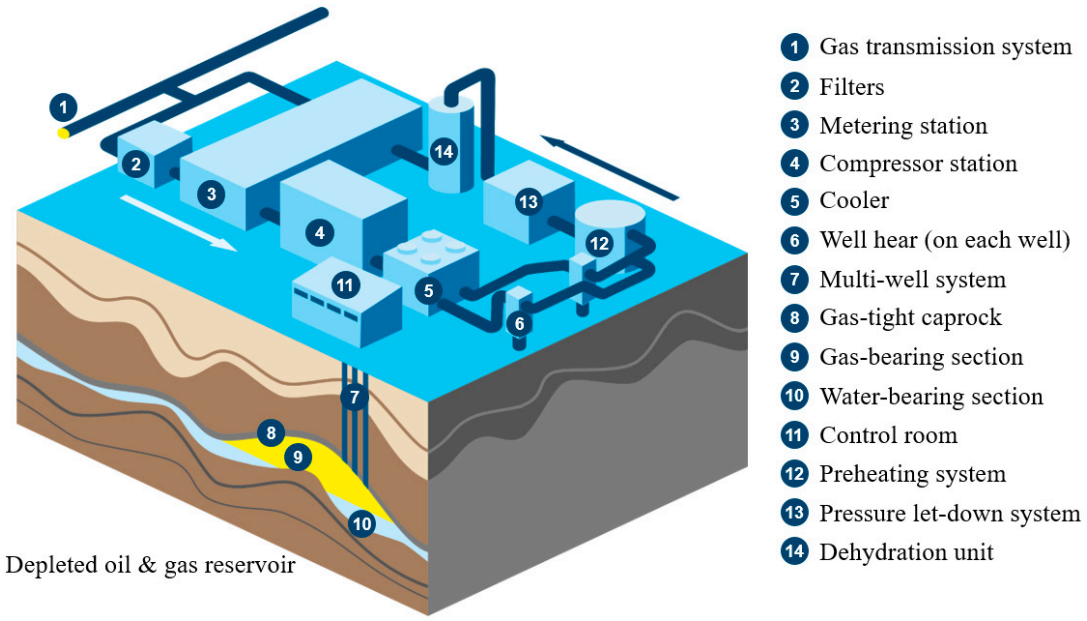

(**a**)

Figure 1. *Cont.*

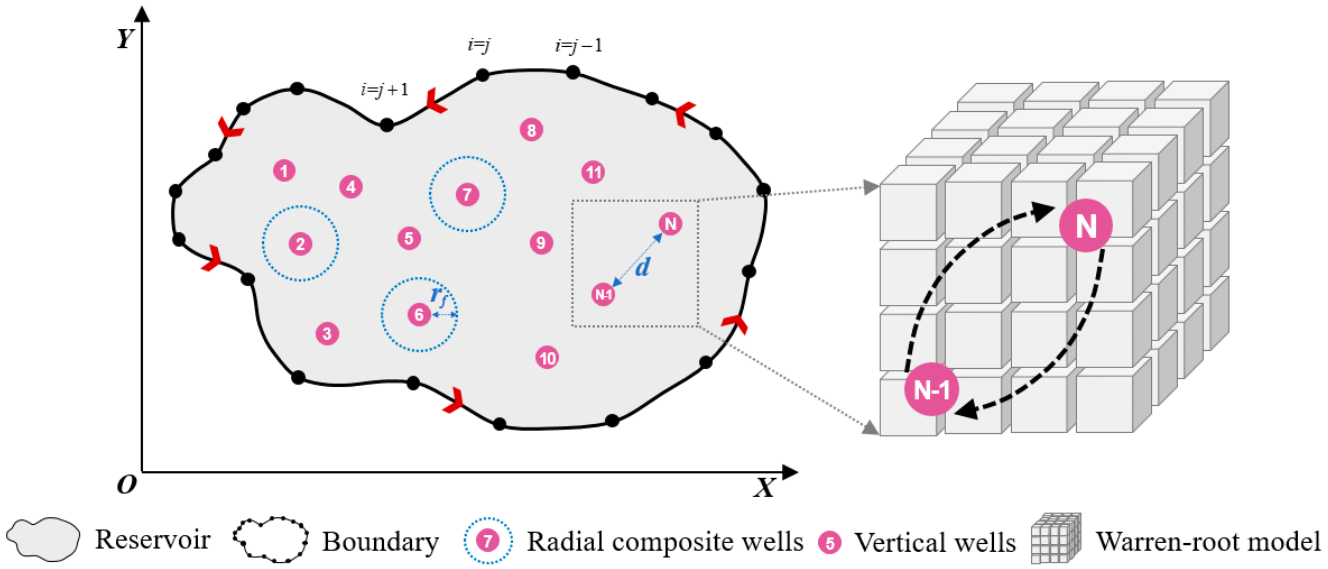

(**b**)

Figure 1. Physical model of the multi-well system with well interference in UGS. (**a**) Schematic diagram (modified from Uniper [31]); (**b**) the multi-well system and reservoir media.

2.2. Mathematical Model

Using the definitions of dimensionless variables in the Appendix A, the continuity equation for a multi-well system in UGS can be written as

$$\frac{d^2\overline{m}_D}{dr_D^2} + \frac{1}{r_D}\frac{d\overline{m}_D}{dr_D} = u\frac{d\overline{m}_D}{dt_D} \tag{1}$$

where $\overline{m}_D$ is the dimensionless pseudo-pressure in the Laplace domain, t_D is the dimensionless time, r_D is the dimensionless distance, and u refers to the Laplace variable. The initial condition for the multi-well system can be written as

$$m_D(r_D, t_D)_{t_D \to 0} = 0 \tag{2}$$

The inner boundary condition including skin factor and wellbore storage effect is

$$C_D u\overline{m}_{wD} - r_D\frac{d\overline{m}_D}{dr_D}_{r_D=1} = \frac{1}{u} \tag{3}$$

$$\overline{m}_{wD} = \left[\overline{m}_D - S\frac{d\overline{m}_D}{dr_D}\right]_{r_D=1} \tag{4}$$

where C_D is the wellbore storage coefficient, S is the skin factor, and $\overline{m}_{wD}$ is the dimensionless bottom-hole pseudo-pressure. The condition for the irregular closed outer boundary is

$$m_D(r_D, t_D)_{r_D \to \infty} = 0 \tag{5}$$

The solution for the homogeneous model with wellbore storage and skin factor is

$$\overline{m}_{wD} = \frac{K_0\left(\sqrt{f(u)}\right) + S\sqrt{f(u)}K_1\left(\sqrt{f(u)}\right)}{f(u)\left\{\sqrt{f(u)}K_1\left(\sqrt{f(u)}\right) + C_D f(u)\left[K_0\left(\sqrt{f(u)}\right) + S\sqrt{f(u)}K_1\left(\sqrt{f(u)}\right)\right]\right\}} \tag{6}$$

where K_0 refers to the zero-order first-class Bessel function and K_1 is the first-order first-class Bessel function. For a heterogeneous reservoir, Equation (1) for the inner and outer regions can be written as

$$\frac{d^2\overline{m}_{1D}}{dr_D^2} + \frac{1}{r_D}\frac{d\overline{m}_{1D}}{dr_D} = u\frac{d\overline{m}_{1D}}{dt_D} \tag{7}$$

$$\frac{d^2\overline{m}_{2D}}{dr_D^2} + \frac{1}{r_D}\frac{d\overline{m}_{2D}}{dr_D} = \frac{\omega_{12}}{M_{12}}u\frac{d\overline{m}_{2D}}{dt_D} \tag{8}$$

The inner boundary condition is

$$C_D u\overline{m}_{wD} - r_D\frac{d\overline{m}_{1D}}{dr_D}_{r_D=1} = \frac{1}{u} \tag{9}$$

$$\overline{m}_{wD} = \left[\overline{m}_{1D} - S\frac{d\overline{m}_{1D}}{dr_D}\right]_{r_D=1} \tag{10}$$

The boundary conditions for the inner and outer regions are

$$\overline{m}_{1D}|_{r_D=r_{fD}} = \overline{m}_{2D}|_{r_D=r_{fD}} \tag{11}$$

$$\left.\frac{d\overline{m}_{1D}}{dr_D}\right|_{r_D=r_{fD}} = \frac{1}{M_{12}}\left.\frac{d\overline{m}_{2D}}{dr_D}\right|_{r_D=r_{fD}} \tag{12}$$

where the subscripts 1 and 2 represent the inner and outer regions, r_{fD} is the composite radius, and M_{12} is the mobility ratio. The outer boundary condition for the outer region is

$$m_{2D}(r_D, t_D)_{r_D\to\infty} = 0 \tag{13}$$

Thus, the radial composite model solution with wellbore storage and skin is

$$\overline{m}_{wD} = \frac{1}{u}\frac{1 + S \times R_D}{R_D + C_D u[1 + S \times R_D]} \tag{14}$$

where

$$R_D = I_{12} \times \sqrt{u}\frac{KI \times KI_1 - 1}{KI \times KI_0 + 1} \tag{15}$$

$$I_{12} = \frac{I_1(\sqrt{u})}{I_0(\sqrt{u})} \tag{16}$$

$$KI_0 = \frac{K_0(\sqrt{u})}{I_0(\sqrt{u})} \tag{17}$$

$$KI_1 = \frac{K_1(\sqrt{u})}{I_0(\sqrt{u})} \tag{18}$$

$$KI = \frac{I_1(a)K_0(b) + \frac{\sqrt{x_{21}}}{M_{12}}I_0(a)K_1(b)}{K_1(a)K_0(b) - \frac{\sqrt{x_{21}}}{M_{12}}K_0(a)K_1(b)} \tag{19}$$

$$a = r_{fD}\sqrt{u} \tag{20}$$

$$b = r_{fD}\sqrt{x_{21}u} \tag{21}$$

$$x_{21} = \frac{\omega_{12}}{M_{12}} \tag{22}$$

where I_0 is the zero-order second-class Bessel function, I_1 is the first-order second-class Bessel function, and ω_{12} is the dispersion ratio. According to pressure superposition, the linear point source function method is chosen to consider the effect of adjacent wells (Ozkan and Raghavan [32]). The point source solution for the i-th offset well is

$$\overline{m}_{D,i} = \overline{q}_{D,i} K_0\left(\sqrt{f(u)} r_{D,i}\right) \tag{23}$$

where $-q_D$ refers to injection. For the Warren–Root model, $f(u)$ is

$$f(u) = \frac{wu(1-w)+\lambda}{u(1-w)+\lambda} \tag{24}$$

where λ is the interporosity flow coefficient and w is the storativity ratio. The tested well location in the multi-well system is considered to be the origin, and the dimensionless distance in Equation (23) is

$$r_{D,i} = \sqrt{(x_{D,i} - x_{wD})^2 + (y_{D,i} - y_{wD})^2} \tag{25}$$

Well interference can be treated with pressure superposition:

$$\overline{m}_{D,j} = \sum_{i=1}^{N} \overline{q}_{D,i} K_0\left(\sqrt{f(u)} r_{D,i,j}\right), j = 2,3,4 \ldots N \tag{26}$$

where N is the number of wells in the multi-well system, and the subscripts i and j represent the serial numbers. The bottom-hole pressure solution with the interference of offset wells is

$$\overline{m}_{wD,Final} = \overline{m}_{wD} + \overline{m}_{D,j} \tag{27}$$

We obtain the bottom-hole pressure in the time domain using the Stehfest numerical inversion algorithm (Stehfest [33]).

3. Method Verification

3.1. Homogeneous Model

Figures 2 and 3 compare pressure and pressure derivative results from a numerical simulator and the proposed model. In case 1 of the homogeneous model verification, the multi-well system includes two production wells. The tested well is producing at a constant production rate of 1 m^3/day. An adjacent well, 50 m from the tested well, is producing at the same constant production rate. In contrast, the adjacent well in case 2 is completing the gas injection process with the same injection rate. The reservoir boundary is set to infinity in two cases. The remaining input parameters of the two cases are shown in Table 3. As the offset well interferes with the testing process of the tested well, Figure 2 shows that the pressure derivative rises at later times and eventually stabilizes at a higher level. When the adjacent well is an injector, the derivative for the tested well in Figure 3 shows a continuous decrease, similar to the effect of a constant pressure boundary. The good agreement between the proposed model and the numerical model in Figures 2 and 3 shows that the proposed model is reliable.

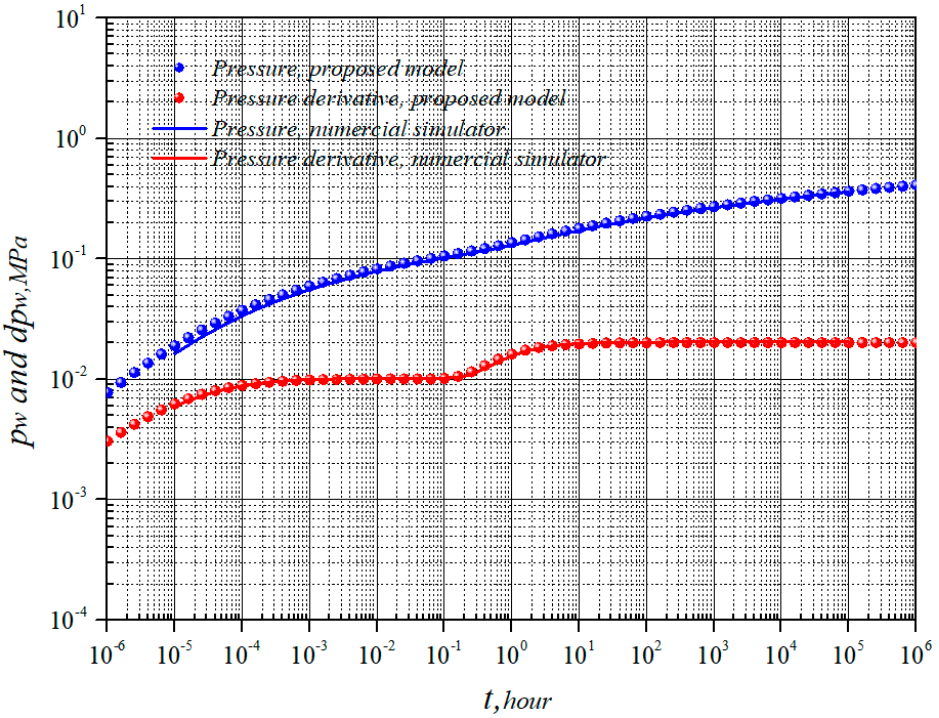

Figure 2. Comparison of the proposed model and numerical simulator for the homogeneous model case 1.

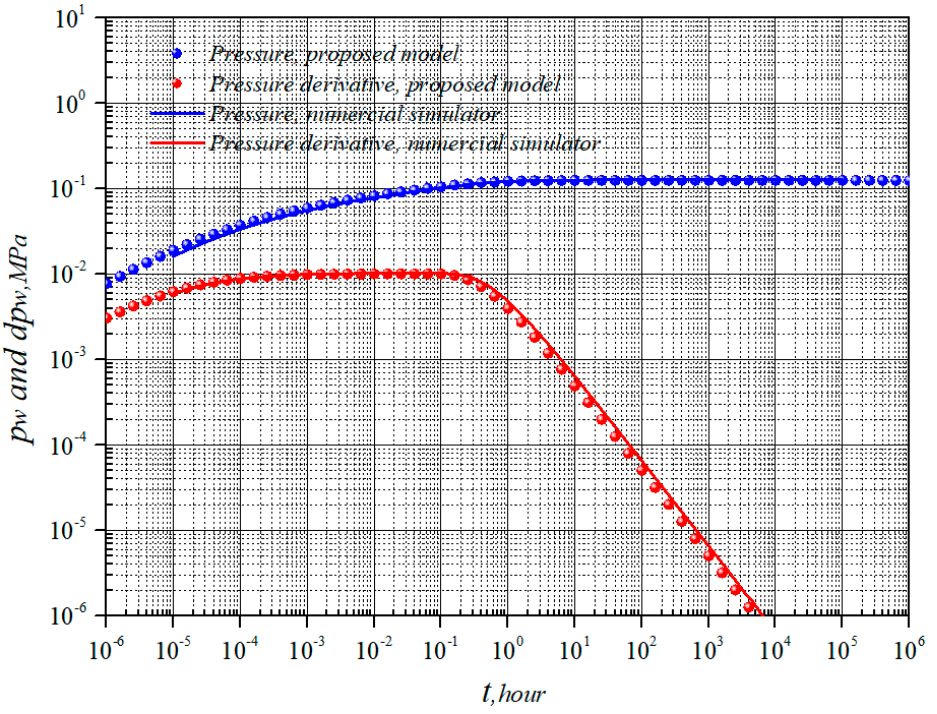

Figure 3. Comparison of the proposed model and numerical simulator for homogeneous model case 2.

Table 3. The reservoir, well, and gas properties in the method verification.

Group	Item	Case 1	Case 2	Case 3	Unit
Reservoir	Initial pressure	34.47	34.47	34.47	MPa
	Reservoir permeability	10	10	10	md
	Reservoir thickness	9.144	9.144	9.144	m
	Porosity	0.1	0.1	0.1	/
	Total compressibility	4.35×10^{-4}	4.35×10^{-4}	4.35×10^{-4}	MPa^{-1}
	Well spacing	50	50	500	m
	Mobility ratio	/	/	4	/
	Dispersion ratio	/	/	1	/
	Composite distance	/	/	100	m
Well	Tested well rate	1	1	1	m^3/day
	Adjacent well rate	1	−1	1	m^3/day
	Well radius	0.09	0.09	0.09	m
	Skin factor	0	0	0	/
	Wellbore storage coefficient	0	0	0	m^3/MPa
Gas	Viscosity	0.02	0.02	0.02	mpa.s
	Z-factor	0.0192	0.0192	0.0192	/

3.2. Radially Composite Model

Pressure transient testing results show that the continuous gas injection process in the UGS usually leads us to conclude that the formation is heterogeneous. Therefore, the radially composite model we used to describe the heterogeneous features is also appropriate for verification. We modeled the tested wells and adjacent wells in a multi-well system considered as a radially composite system and as a homogeneous system. The mobility ratio and dispersion ratio between the inner and outer regions were chosen as 4 and 1, as given in Table 4. The composite radius was initially chosen to be 100 m. The well spacing between the offset well and the tested well was selected as 500 m, and both wells produced at a constant rate of 1 m^3/day. The pressure derivative curve in Figure 4 shows that the derivative will eventually stabilize at a higher level, which may be related to the adjacent well interference and formation heterogeneity.

Table 4. The sequence, name, and feature of typical flow regimes in UGS.

Sequence	Name	Feature
(a)	Wellbore storage effect	Straight line with unit slope
(b)	Skin factor effect	Hump
(c)	Radial flow within the inner zone	Constant value of 0.5
(d)	Transitional flow	/
(e)	Radial flow in the outer region	Constant value of 0.5 × M
(f)	Transitional flow	/
(g)	Radial flow with well interference	Constant value of $0.5 \times M \times Q_{test,D} + Q_{adj,D} \times 0.5$

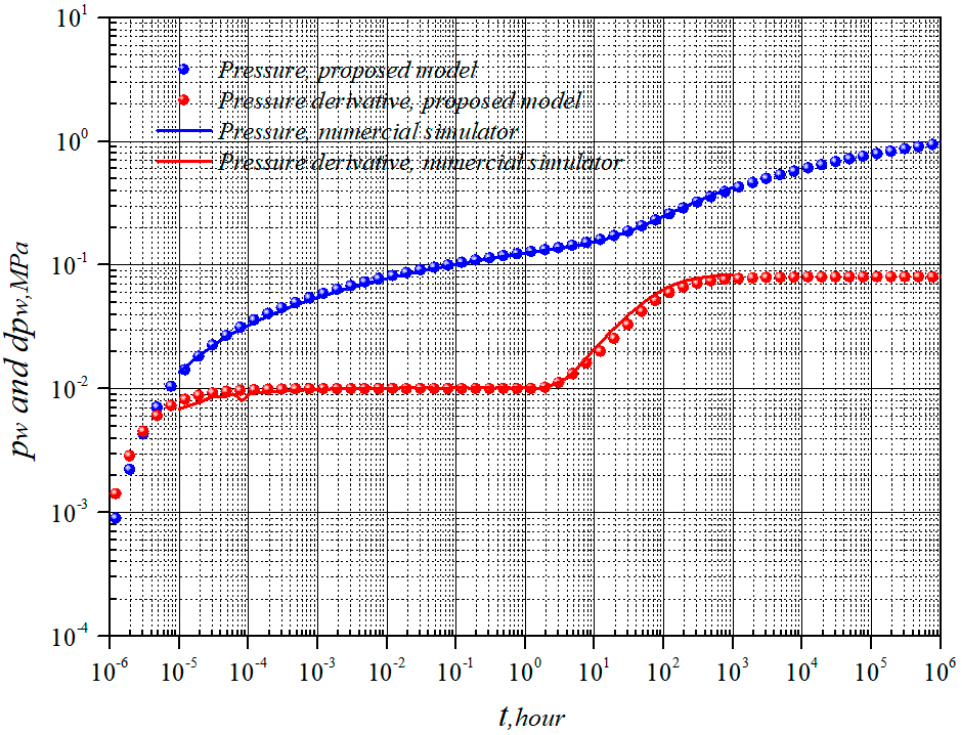

Figure 4. Comparison of the proposed model and numerical simulator for a radially composite model.

4. Results and Discussion

4.1. Flow Regimes

Figure 5 and Table 4 show that wellbore storage dominates the first flow regime. Due to the difference between the production rate at the wellhead and the well bottom, the pressure and its derivative both fall on a straight line with unit slope. The pressure derivative that follows exhibits the effect of a skin factor and includes a hump. The height of the hump is related to the wellbore storage coefficient C_D and the skin factor S. The third stage indicates radial flow within the inner zone, as the pressure derivative curve appears as a horizontal line with a value of 0.5. As the pressure response continues to propagate, the transition between the inner and outer regions begins gradually. When the pressure response propagating to the outer zone gradually becomes circular, radial flow in the outer region begins to appear. At this stage, the pressure derivative appears as a straight line, and its value is related to the ratio between 0.5 and the mobility ratio. After the radial flow in the outer region, the features of offset well interference gradually appear. The pressure derivative begins to rise continuously, indicating transitional flow. As well interference gradually increases, the characteristics of the entire multi-well system gradually appear. Finally, radial flow appears in the multi-well system. At this time, the horizontal derivative curve during radial flow of the multi-well system can be divided into two parts: the radial composite feature of the tested well and the adjacent well interference. The radially composite feature results in the horizontal line values related to 0.5, mobility ratio, and dimensionless production rate of the tested well. Well interference also causes the horizontal line value to relate to the dimensionless production rate of the offset well and 0.5. If offset wells are in the process of gas injection, the pressure derivative shows the characteristic of drop-off. The comparison of the newly added single-well model in Figure 5 shows that the pressure derivative of the single-well model finally stabilizes at the horizontal line with the value of 0.5 M.

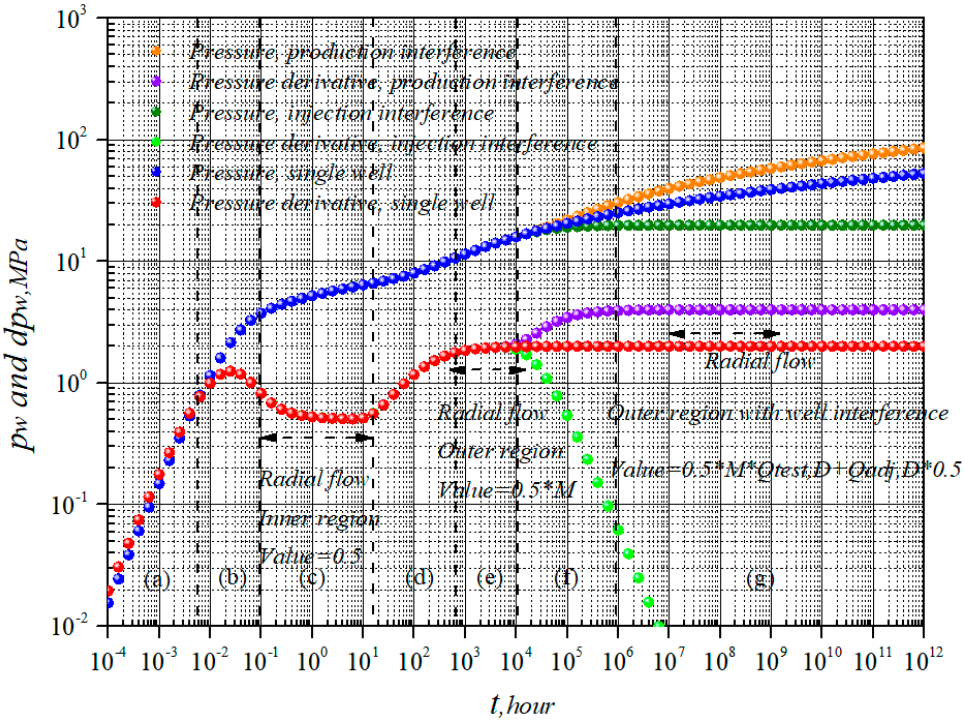

Figure 5. Flow regimes in the multi-well system with a radially composite reservoir and well interference during UGS. The pressure behaviors of the single well model are used for comparison.

4.2. Sensitivity Analysis

4.2.1. Effect of Well Spacing

Figure 6 shows the effect of well spacing on the pressure transient behavior of tested wells in the multi-well system as well spacing is gradually increased from 100 m to 5000 m. We can draw the conclusion that the variation of well spacing affects the radial flow regime in the inner region, the transitional flow between the inner and the outer regions, the radial flow in the outer region, and the pseudo-radial flow in the multi-well system. As well spacing increases, the duration of radial flow in the inner region increases gradually. The starting time of the radial flow of the multi-well system is proportional to the well spacing. When the well spacing is 100 m, the tested well and adjacent wells can easily communicate with each other to form a whole. In this case, the flow regimes are simple. Radial flow in the inner region is followed by a long transitional flow regime. This transitional flow is controlled by a combination of radial composite features and well interference. Since the well spacing is the same as the composite radius, the characteristics of well interference mask the radial flow feature of the outer region. The pressure derivative rises. With the gradual increase in well spacing, the transitional flow regime between the inner and outer regions, the radial flow regime in the outer region, and the transitional flow during well interference gradually emerge. As the well spacing increases to 1000 m, the transitional flow between the inner and outer regions begins to appear. When the well spacing increases to 5000 m, the pressure derivative exhibits both radial flow in the outer region and transitional flow that characterizes interference.

4.2.2. Effect of Neighboring Well's Production Rate

Figure 7 shows the effect of adjacent well production changes on the pressure derivative in the multi-well system. The dimensionless production rate of adjacent wells varies from 1 to 5, 10, and 20. A comparison of pressure derivatives shows that interference from adjacent well production affects the transition flow region of the test well and the pseudo-radial flow region of the multi-well system. As the production rate of adjacent wells increases, the slope of the pressure derivative curve increases gradually during the

well interference transition flow regime. The pressure derivative curve also displays a horizontal line in the pseudo-radial flow regime of the multi-well system, and its value is proportional to the production rate of the adjacent well. Flow regime analysis shows that rate variation in adjacent wells affects the pseudo-radial flow during interference within the multi-well system.

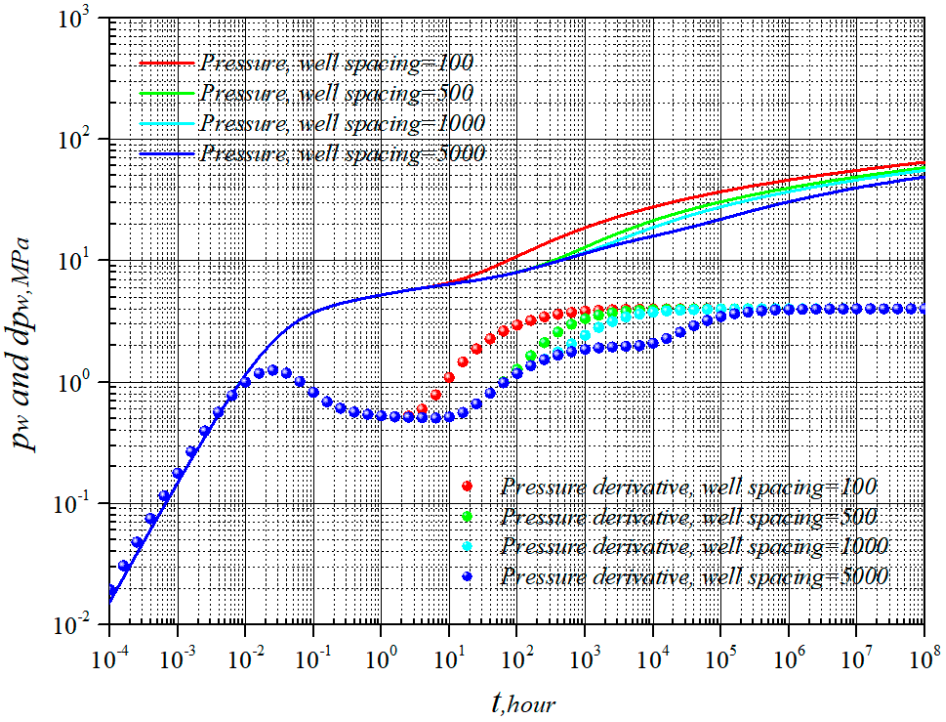

Figure 6. Effect of well spacing on the tested well's pressure behaviors in the multi-well system.

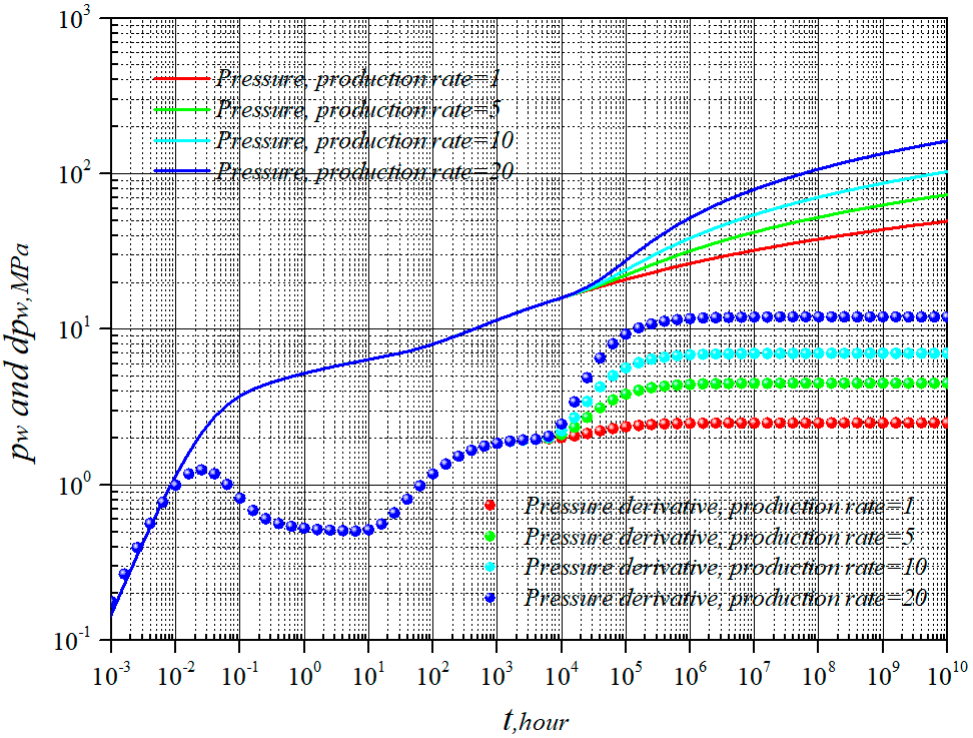

Figure 7. Effect of neighboring well's production rate on the tested well's pressure behaviors in the multi-well system.

4.2.3. Effect of Neighboring Well's Injection Rate

The effect of the neighboring well's injection rate on the pressure of the tested wells in a multi-well system is shown in Figure 8. The dimensionless neighbor well's injection rate increased from 1 to 6. An example of a neighbor well producing at a constant production rate is also shown for comparison. A comparison of pressure derivatives shows that the neighbor well affects the well interference transition flow regime and the pseudo-radial flow of the multi-well system. With the increase in the injection rate of adjacent wells, the rise of the pressure curve slows and the pressure derivative curve gradually rises to a lower horizontal level during pseudo-radial flow in the multi-well system. The tested well's dimensionless production rate is 1, and the mobility ratio between various regions is 4. As the dimensionless production rate of neighboring wells increases to 4, the pressure curve does not rise, and the derivative curve begins to trend downward. This downward trend becomes more pronounced as the injection rate into adjacent wells increases.

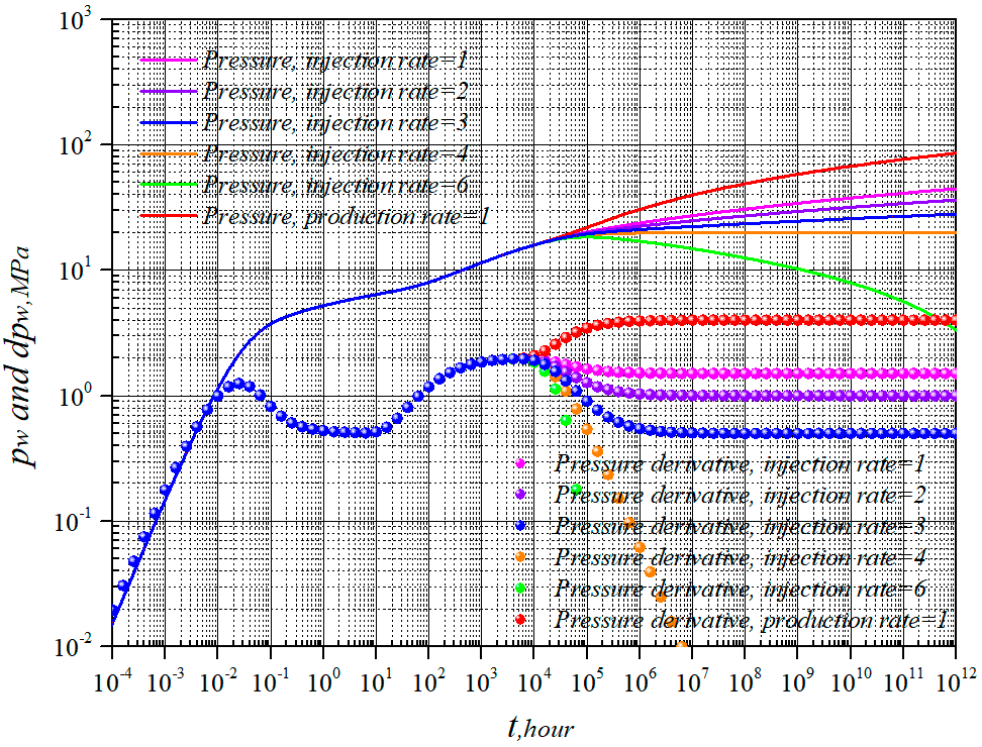

Figure 8. Effect of neighbor well's injection rate on the tested well's pressure behaviors in the multi-well system.

4.2.4. Effect of Composite Radius

The effect of composite radius changes on tested wells in a multi-well system is shown in Figure 9. The composite radius of the test well is gradually increased from 100 m to 500 m. The comparison of the pressure derivative curves in Figure 9 shows that the change of composite radius affects the radial flow in the inner region, the transitional flow between various regions, and the radial flow in the outer region. As the composite radius increases, the radial flow duration in the inner region gradually increases, and the starting and ending times of the transitional flow in the inner and outer regions are gradually delayed. As a result, radial flow in the outer region is masked. Both transitional flow in the inner and outer regions and radial flow in the outer region have the characteristics of the transitional flow.

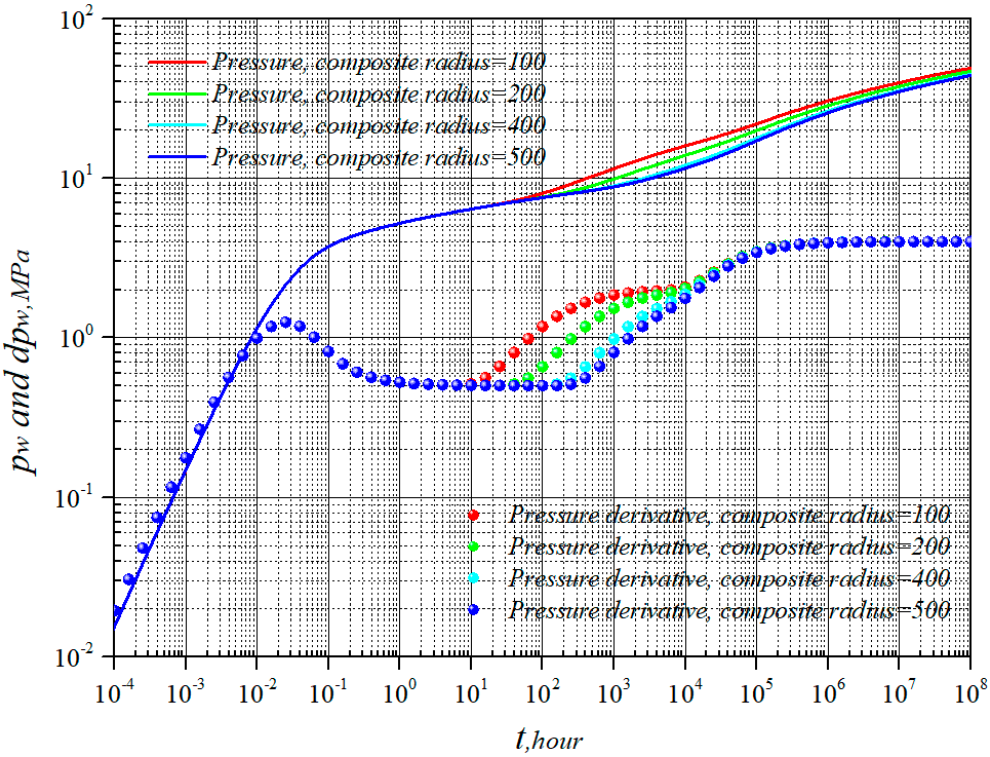

Figure 9. Effect of composite radius on the tested well's pressure behaviors in the multi-well system.

5. Field Application

5.1. Geological Background

Hutubi UGS is located in the southern margin of the Junggar Basin (piedmont depression of north Tianshan Mountain), as shown in Figure 10. It is a long axis anticline with an east–west direction of about 20 km in length and 3.5 km in width from north to south. It was cut along the long axis by two nearly parallel overthrust faults (Hutubi fault and Hutubi North fault). The gas layer of the Ziniquanzi Formation is a set of regressive delta deposits, about 355 m thick. The lithology is mainly brown, grayish-brown fine sandstone, unequal-grained sandstone, siltstone, pebbled unequal-grained sandstone, and pebbled argillaceous sandstone, and it has good sealing and trapping conditions. Before the UGS formed, it was a sandstone condensate reservoir with edge and bottom water. Geological data show that the average porosity is 20.9%, the permeability is 62.49 mD, and the original formation pressure is 33.96 MPa. The designed capacity of Hutubi gas storage is 107 $\times$ 10^8 m^3, and the working gas volume is 45.1 $\times$ 10^8 m^3.

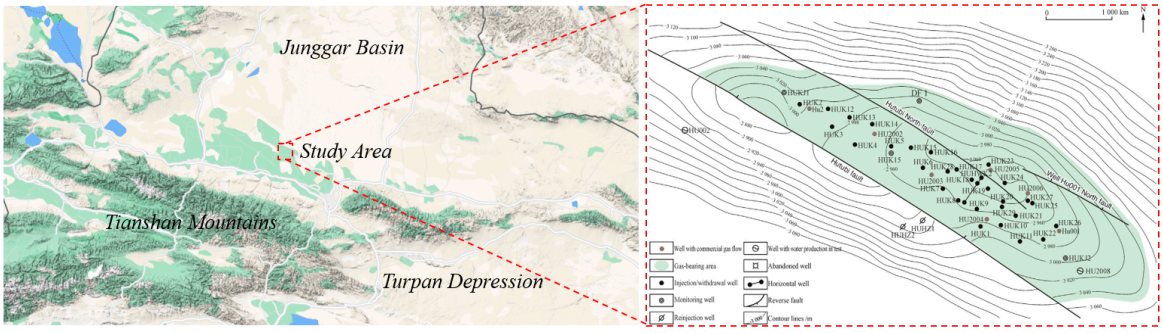

(**a**) (**b**)

Figure 10. (**a**) Regional location of the study area. (**b**) Structure and well location map of the study area (modified from Zheng et al. [34]).

5.2. Pressure Transient Testing

As shown in Figure 10b, two wells in the UGS were selected for pressure transient testing. The target well (a) is in the fourth cycle of cumulative gas injection of 4970.46 $\times$ 10^4 m^3 before the pressure transient testing, and the daily gas injection rate is stable at 21.67 $\times$ 10^4 m^3/day. The pressure gauge was lowered to the well bottom hole of 3463 m on 31 August 2016, and the duration of the pressure transient test was 20 days. During testing, gas injection into the offset well began with varying rates. The cumulative gas injection into the target well (b) in the fourth cycle before the test was 10,580 $\times$ 10^4 m^3, and the daily gas injection rate was stable at 68.68 $\times$ 10^4 m^3/day. On 24 September 2016, the pressure gauge was lowered to the bottom hole at 3472 m, and the cumulative test duration was 19 days. During the test period, gas was injected into the adjacent well (a) at an average rate of 24.4341 $\times$ 10^4 m^3/day from 23 September to 1 October. Gas was injected into the adjacent well (b) from 24 September to 1 October at an average gas injection rate of 27.24 $\times$ 10^4 m^3/day. The pressure testing data in Figures 11 and 12 show that the derivatives decrease, and the difference between target wells (a) and (b) is that the test period is different. For target well (a), the impact time of falling down is the ending period of the pressure derivative. This test time for target well (b) is in the middle and late stages of the derivative curve. Combining the test period of the target well with the production period of the adjacent wells, we can draw the conclusion that there are well interference and formation heterogeneity. The single-well models in Figures 11 and 12 could not match the later stage of actual data. Further, we used the proposed model to match the field data and compared pressures and derivatives in Figures 11 and 12 which illustrate the applicability of the model. The reservoir, well, and gas properties are provided in Tables 5 and 6.

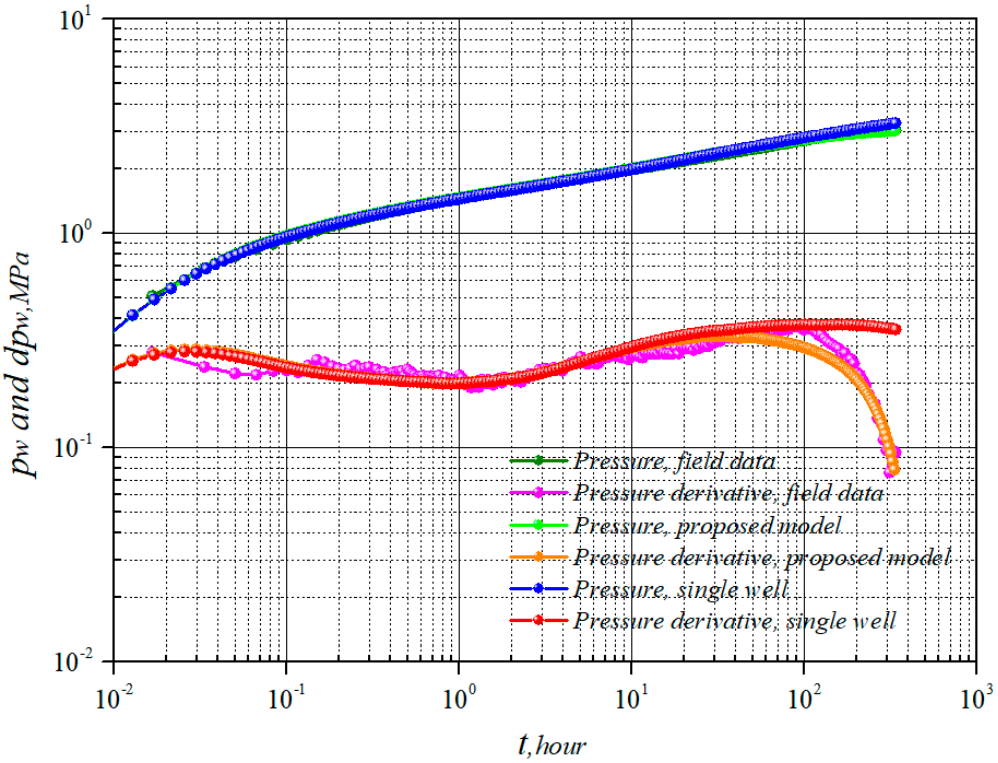

Figure 11. Pressure and pressure derivative match results in the fourth cycle of cumulative gas injection for case 1.

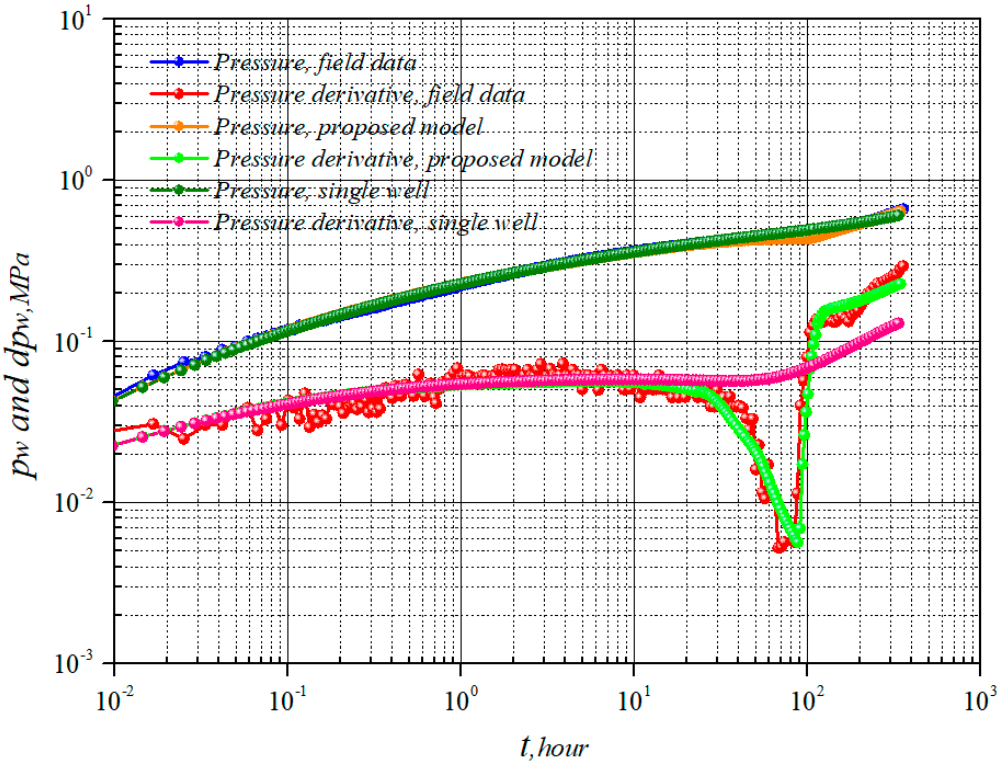

Figure 12. Pressure and pressure derivative match results in the fourth cycle of cumulative gas injection for case 2.

Table 5. The reservoir, well, and gas properties in pressure transient analysis of case 1.

Group	Item	Value	Unit
Reservoir	Initial pressure	29.47	MPa
	Reservoir permeability	4.31	md
	Reservoir thickness	35	m
	Porosity	0.2	
	Total compressibility	4.35×10^{-4}	MPa^{-1}
	Mobility ratio	2.1	
	Dispersion ratio	2.2	
	Composite distance	28	m
	Well spacing	300	m
Well	Adjacent well rate	1×10^6	m^3/day
	Well radius	0.1	m
	Skin factor	−1.37	
	Wellbore storage coefficient	0.63	m^3/MPa
Gas	Viscosity	0.02	mpa.s
	Z-factor	0.0192	

Table 6. The reservoir, well, and gas properties in pressure transient analysis of case 2.

Group	Item	Value	Unit
Reservoir	Initial pressure	32.45	MPa
	Reservoir permeability	70	md
	Reservoir thickness	22	m
	Porosity	0.2	
	Total compressibility	4.35×10^{-4}	MPa^{-1}
	Mobility ratio	10	
	Dispersion ratio	10	
	Composite distance	830	m
	Well spacing	470	m
Well	Adjacent well rate	5×10^5	m^3/day
	Well radius	0.1	m
	Skin factor	−4.75	
	Wellbore storage coefficient	0.15	m^3/MPa
Gas	Viscosity	0.02	mpa.s
	Z-factor	0.019	

6. Summary and Conclusions

This work uses an analytical approach to analyze the pressure transient behavior of a multi-well system in UGS. The model reliability was validated with a commercial numerical simulator. Typical flow regimes in UGS were diagnosed using Bourdet pressure derivatives. Sensitivity analysis and the field case from Hutubi UGS demonstrate the practical applicability of the method. Some key conclusions are as follows:

1. The typical flow regimes for a vertical well in the UGS include wellbore storage, skin effect, radial flow in an inner region, radial flow in an outer region, and effects of well interference.

2. Long-duration gas injection and production periods in the UGS amplify the influence of heterogeneities in a formation. With an increase in gas injection and production, heterogeneities exhibited by the reservoir increase, and the radially composite signature in the pressure transient test response becomes more apparent. The pressure derivative increases in the middle and later periods.

3. The typical signature of the flow regime during which well interference occurs depends on the operation of adjacent wells. As adjacent wells are producing, the pressure derivative finally exhibits the pseudo-radial flow of the multi-well system under the influence of well interference. The horizontal derivative value is related to the dimensionless production rate of the target well, adjacent wells, mobility ratio, and 0.5. When injection into adjacent wells is occurring, the final portion of the pressure derivative curve decreases.

4. Field application shows that well interference and formation heterogeneity are commonly observed in UGS, and the pressure derivative curve tends to have rising and falling features. The proposed model can be used to effectively analyze the transient pressure data with well interference and heterogeneity in the UGS.

This is our primary work on UGS. The study focuses on the pressure behavior of multiple vertical wells. Our future research work will be extended to complex situations of various well types, pressures, and rate behaviors. In addition, more UGS field data will be collected to form a multidisciplinary approach.

Author Contributions: Conceptualization, H.C. and T.M.; methodology, H.C.; software, Y.G.; validation, Y.G.; formal analysis, Z.C.; investigation, Z.C.; resources, W.L.; data curation, H.C.; writing—original draft preparation, H.C.; writing—review and editing, H.C.; visualization, H.C.; supervision, W.L.; project administration, T.M.; funding acquisition, H.C. All authors have read and agreed to the published version of the manuscript.

Funding: This research was funded by National Science Foundation, China (12202042); China Postdoctoral Science Foundations (2021M700391); and Fundamental Research Funds for the Central Universities (QNXM20220011). And The APC was funded by Fundamental Research Funds for the Central Universities (QNXM20220011).

Conflicts of Interest: The authors declare no conflict of interest.

Nomenclature

k	permeability, D
m_D	dimensionless pseudo-pressure pressure
t_D	dimensionless time
r_D	dimensionless distance
u	Laplace variable
C_D	wellbore storage coefficient
S	skin factor
m_{wD}	dimensionless bottom-hole pseudo-pressure
K_0	zero-order first-class Bessel function
K_1	first-order first-class Bessel function
r_{fD}	dimensionless composite radius
M_{12}	mobility ratio
ω_{12}	dispersion ratio
I_0	zero-order second-class Bessel function
I_1	first-order second-class Bessel function
λ	interporosity flow coefficient
ω	storativity ratio
N	well number
μ	viscosity, mpa.s
B	formation volume factor
h	thickness, m
C_t	total compressibility, MPa^{-1}
L	reference length, m
φ	porosity
d	well spacing, m
q	production rate, m^3/day
T	temperature, K
T_{sc}	temperature at standard conditions, K
p_{sc}	pressure at standard conditions, MPa

Appendix A. Dimensionless Variables

Dimensionless pseudo-pressure in UGS,

$$m_D = \frac{kT_{sc}h(m_i - m)}{3.684 \times 10^{-3} p_{sc} q_{t,sc} T} \tag{A1}$$

where

$$m = \int_{p_{sc}}^{p} \frac{p}{\mu Z} dp \tag{A2}$$

Dimensionless time,

$$t_D = \frac{3.6kt}{\mu \Lambda h^2} \tag{A3}$$

where

$$\Lambda = \varphi C_g + \frac{kh}{1.842 \times 10^{-3} q_{sc} \mu} \tag{A4}$$

Dimensionless wellbore storage coefficient,

$$C_D = \frac{0.159C}{\varphi C_t h L^2} \tag{A5}$$

Dimensionless well spacing,

$$d_D = \frac{d}{L} \tag{A6}$$

Dimensionless mobility ratio,

$$M_{12} = \frac{(k/u)_1}{(k/u)_2} \tag{A7}$$

Dimensionless dispersion ratio,

$$\omega_{12} = \frac{(\varphi C_t)_1}{(\varphi C_t)_2} \tag{A8}$$

Dimensionless distance,

$$x_D = \frac{x}{L}, y_D = \frac{y}{L}, r_D = \frac{r}{L} \tag{A9}$$

Dimensionless location for the origin,

$$x_{wD} = \frac{x_w}{L}, y_{wD} = \frac{y_w}{L}, r_{wD} = \frac{r_w}{L} \tag{A10}$$

References

1. Yang, C.; Wang, T.; Li, Y.; Yang, H.; Li, J.; Qu, D.; Xu, B.; Yang, Y.; Daemen, J. Feasibility analysis of using abandoned salt caverns for large-scale underground energy storage in China. *Appl. Energy* **2015**, *137*, 467–481. [CrossRef]
2. Matos, C.R.; Carneiro, J.F.; Silva, P.P. Overview of large-scale underground energy storage technologies for integration of renewable energies and criteria for reservoir identification. *J. Energy Storage* **2019**, *21*, 241–258. [CrossRef]
3. Jensen, J.H.; Poulsen, J.M.; Andersen, N.U. From coal to clean energy. *Nitrogen Syngas* **2011**, *310*, 34–38.
4. Weijermars, R.; Drijkoningen, G.; Heimovaara, T.J.; Rudolph, E.S.J.; Weltje, G.J.; Wolf, K.H.A.A. Unconventional gas research initiative for clean energy transition in Europe. *J. Nat. Gas Sci. Eng.* **2011**, *3*, 402–412. [CrossRef]
5. Qyyum, M.A.; Naquash, A.; Haider, J.; Al-Sobhi, S.A.; Lee, M. State-of-the-art assessment of natural gas liquids recovery processes: Techno-economic evaluation, policy implications, open issues, and the way forward. *Energy* **2022**, *238*, 121684. [CrossRef]
6. Zhang, J.; Tan, Y.; Zhang, T.; Yu, K.; Wang, X.; Zhao, Q. Natural gas market and underground gas storage development in China. *J. Energy Storage* **2000**, *29*, 101338. [CrossRef]
7. Chen, J.; Yu, J.; Ai, B.; Song, M.; Hou, W. Determinants of global natural gas consumption and import–export flows. *Energy Econ* **2019**, *83*, 588–602. [CrossRef]
8. Crow, D.J.; Giarola, S.; Hawkes, A.D. A dynamic model of global natural gas supply. *Appl. Energy* **2018**, *218*, 452–469. [CrossRef]
9. Demirel, N.Ç.; Demirel, T.; Deveci, M.; Vardar, G. Location selection for underground natural gas storage using Choquet integral. *J. Nat. Gas Sci. Eng.* **2017**, *45*, 368–379. [CrossRef]
10. Wang, J.; Zhang, J.; Xie, J.; Ding, F. Initial gas full-component simulation experiment of Ban-876 underground gas storage. *J. Nat. Gas Sci. Eng.* **2014**, *18*, 131–136. [CrossRef]
11. Wang, J.; Feng, X.; Wanyan, Q.; Zhao, K.; Wang, Z.; Pei, G.; Xie, J.; Tian, B. Hysteresis effect of three-phase fluids in the high-intensity injection–production process of sandstone underground gas storages. *Energy* **2022**, *242*, 123058. [CrossRef]
12. Lv, J.; Li, Z.; Fu, J.; Tang, J.; Wei, X.; Qie, X. Compositional variation laws of produced gas from underground gas storage tanks rebuilt from sour gas reservoirs: A case study of Shaan 224 UGS in the Ordos Basin. *Nat. Gas Ind.* **2017**, *37*, 96–101.
13. Tang, Y.; Long, K.; Wang, J.; Xu, H.; Wang, Y.; He, Y.; Shi, L.; Zhu, H. Change of phase state during multi-cycle injection and production process of condensate gas reservoir based underground gas storage. *Pet. Explor. Dev.* **2021**, *48*, 395–406. [CrossRef]
14. Lewandowska-Śmierzchalska, J.; Tarkowski, R.; Uliasz-Misiak, B. Screening and ranking framework for underground hydrogen storage site selection in Poland. *Int. J. Hydrogen Energy* **2018**, *43*, 4401–4414. [CrossRef]

15. Cedigaz. Underground Gas Storage in the World—2017 Status. 2017. Available online: http://www.cedigaz.org/resources/free-downloads.aspx/ (accessed on 1 March 2018).
16. Lee, J. Well testing. *Soc. Pet. Eng.* **1982**.
17. Meehan, D.N.; Horne, R.N.; Ramey, H.J. Interference testing of finite conductivity hydraulically fractured wells. In Proceedings of the SPE Annual Technical Conference and Exhibition, San Antonio, TX, USA, 8 October 1989.
18. Malekzadeh, D.; Tiab, D. Interference testing of horizontal wells. In Proceedings of the SPE Annual Technical Conference and Exhibition, Dallas, TX, USA, 6–9 October 1991.
19. Awotunde, A.A.; Al-Hashim, H.S.; Al-Khamis, M.N.; Al-Yousef, H.Y. Interference Testing Using Finite-Conductivity Horizontal Wells of Unequal Lengths. In Proceedings of the SPE Eastern Regional/AAPG Eastern Section Joint Meeting, Pittsburgh, PA, USA, 11–15 October 2008.
20. Al-Khamis, M.; Ozkan, E. Analysis of interference tests with horizontal wells. *SPE Res. Eval. Eng.* **2005**, *8*, 337–347. [CrossRef]
21. Spivey, J.P.; Lee, W.J. *Applied Well Test Interpretation*; Society of Petroleum Engineers: Richardson, TX, USA, 2013; Volume 13, pp. 187–229.
22. Warren, J.E.; Root, P.J. The behavior of naturally fractured reservoirs. *Soc. Pet. Eng. J.* **1963**, *3*, 245–255. [CrossRef]
23. Onur, M.; Serra, K.V.; Reynolds, A.C. Analysis of pressure-buildup data from a well in a multiwell system. *SPE Form. Eval.* **1991**, *6*, 101–110. [CrossRef]
24. Fokker, P.A.; Verga, F. A semianalytic model for the productivity testing of multiple wells. *SPE Reserv. Eval. Eng.* **2008**, *11*, 466–477. [CrossRef]
25. Lin, J.E.; Yang, H.Z. Analysis of well-test data from a well in a multiwell reservoir with water injection. In Proceedings of the SPE Annual Technical Conference and Exhibition, Anaheim, CA, USA, 11–14 November 2007.
26. Izadi, M.; Yildiz, T. Transient flow in discretely fractured porous media. *SPE J.* **2009**, *14*, 362–373. [CrossRef]
27. Wei, C.; Liu, Y.; Deng, Y.; Cheng, S.; Hassanzadeh, H. Analytical well-test model for hydraulicly fractured wells with multiwell interference in double porosity gas reservoirs. *J. Nat. Gas Sci. Eng.* **2022**, *103*, 104624. [CrossRef]
28. Chu, H.; Liao, X.; Chen, Z.; John Lee, W.J. Rate-transient analysis of a constant-bottomhole-pressure multihorizontal well pad with a semianalytical single-phase method. *SPE J.* **2020**, *25*, 3280–3299. [CrossRef]
29. Chu, H.; Chen, Z.; Liao, X.; Zhao, X.; Lee, W.J. Pressure transient analysis of a multi-horizontal-well pad by a semi-analytical model: Methodology and case study. *J. Pet. Sci. Eng.* **2022**, *208*, 109538. [CrossRef]
30. Du, G.; He, L.; Zhang, G.; Wang, Y.; Zhang, S.; Zhou, N.; Yang, D.; Zhou, X.; He, H.; Lin, J. Well Testing Analysis Method for a Well in Hutubi Multi-well Underground Gas Storage Reservoir. In Proceedings of the International Field Exploration and Development Conference 2017, Chengdu, China, 12 July 2018; Springer: Singapore; pp. 1870–1882.
31. Uniper. 2022. Available online: https://www.uniper.energy/energy-storage-uniper/gas-storage-technology (accessed on 11 December 2021).
32. Ozkan, E.; Raghavan, R. New solutions for well-test-analysis problems: Part 1-analytical considerations (includes associated papers 28666 and 29213). *SPE Form. Eval.* **1991**, *6*, 359–368. [CrossRef]
33. Stehfest, H. Algorithm 368: Numerical inversion of Laplace transforms [D5]. *Commun. ACM* **1970**, *13*, 47–49. [CrossRef]
34. Zheng, Y.; Sun, J.; Qiu, X.; Lai, X.; Liu, J.; Guo, Z.; Wei, H.; Min, Z. Connotation and evaluation technique of geological integrity of UGSs in oil/gas fields. *Nat. Gas Ind. B* **2020**, *7*, 594–603. [CrossRef]